Title	Electron distribution and scattering in InAs films on low-k flexible substrates
Author(s)	Nguyen, Cong Thanh; Shih, Hong-An; Akabori, Masashi; Suzuki, Toshi-kazu
Citation	Applied Physics Letters, 100(23): 232103-1-232103-4
Issue Date	2012-06-05
Type	Journal Article
Text version	publisher
URL	http://hdl.handle.net/10119/12901
Rights	Copyright 2012 American Institute of Physics. This article may be downloaded for personal use only. Any other use requires prior permission of the author and the American Institute of Physics. The following article appeared in Cong Thanh Nguyen, Hong-An Shih, Masashi Akabori and Toshi-kazu Suzuki, Applied Physics Letters, 100(23), 232103 (2012) and may be found at http://dx.doi.org/10.1063/1.4722798
Description	

Electron distribution and scattering in InAs films on low-*k* flexible substrates

Cong Thanh Nguyen, Hong-An Shih, Masashi Akabori, and Toshi-kazu Suzuki[a)]
Center for Nano Materials and Technology, Japan Advanced Institute of Science and Technology (JAIST), 1-1 Asahidai, Nomi, Ishikawa 923-1292, Japan

(Received 17 April 2012; accepted 9 May 2012; published online 5 June 2012)

On low-k flexible substrates, we obtained InAs films with thickness ranging from several hundreds of nm to sub-10-nm, by epitaxial lift-off and van der Waals bonding. Using Hall measurements, we investigated the electron mobility and sheet concentration depending on the InAs film thickness L. In spite of the undoped InAs films, we do not observe electron depletion even for sub-10-nm thickness L, owing to the Fermi level pinning above the conduction band bottom. We observed three regimes of the behavior of the electron mobility μ with decrease in L: almost constant or slightly increasing μ with decrease in L for $\gtrsim 150$ nm, weakly decreasing μ for $150\,\mathrm{nm} \gtrsim L \gtrsim 15$ nm, and more rapidly decreasing μ proportional to L^{γ} with $\gamma \simeq 5$–6 for $L \lesssim 15$ nm. By using Poisson-Schrödinger calculation, we examined the electron distribution in the film depending on L and the associated scattering mechanisms contributing to the behavior of μ, such as phonon, Coulomb, and thickness fluctuation scattering. © *2012 American Institute of Physics*. [http://dx.doi.org/10.1063/1.4722798]

InAs is an important narrow-gap compound semiconductor,[1,2] with potential applications to mid-infrared optical devices,[3] ultra-high-speed electron devices,[4–6] and also interband tunnel devices.[7,8] Heterogeneous integration of such narrow-gap compound semiconductors on foreign host substrates can lead to superior or innovative functionalities, such as optical and ultra-high-frequency signal processing. As a method of the heterogeneous integration, we proposed epitaxial lift-off (ELO) and van der Waals bonding (VWB) of narrow-gap compound semiconductors obtained by lattice-mismatched growth with nano-scale thin sacrificial layers,[9–11] while most studies on ELO-VWB had been restricted to GaAs lattice-matched systems.[12,13] In the previous work, using the ELO-VWB process, we realized InAs films down to $\sim$20 nm thickness bonded on low dielectric constant (low-k) flexible substrates ($k \lesssim 3$) and showed very high electron mobilities.[11] Low-k flexible substrates with extremely high resistivities have advantages for high-speed applications due to low parasitic capacitance and low leakage current, and also are important for light-weight, portable, and flexible electronic apparatus applications. More recently, excellent device performances of InGaAs/InAlAs field-effect transistors (FETs) on flexible substrates[14] and InAs FETs on SiO_2/Si (Refs. 15–17) have been reported. Towards InAs devices with such excellent performance on the low-k flexible substrates, it is important to elucidate the electron transport mechanisms in the InAs films on the flexible substrates. In particular, as shown in the previous work, electron mobility lowering is observed below thickness of $\sim$100–200 nm, which should be investigated.

In this work, using the ELO-VWB process, we fabricated InAs films with thickness ranging from several hundreds of nm to sub-10-nm on low-k flexible substrates. Electron transport properties depending on the InAs film thickness L were investigated by using Hall measurements at room temperature. In spite of the undoped InAs films, we do not observe electron depletion even for sub-10-nm L. We observed three regimes of the behavior of the electron mobility μ with decrease in L: almost constant or slightly increasing μ with decrease in L for $\gtrsim 150$ nm, weakly decreasing μ for $150\,\mathrm{nm} \gtrsim L \gtrsim 15$ nm, and more rapidly decreasing μ for $L \lesssim 15$ nm, where the last regime has been of interest for a long time in the context of thickness fluctuation scattering[18–23] and is of importance for ultra-thin body devices.[24,25] In order to elucidate the electron transport, we examined the electron distribution in the film depending on L by employing Poisson-Schrödinger calculation and the associated electron scattering mechanisms, such as phonon, Coulomb, and thickness fluctuation scattering.

By means of molecular beam epitaxy, we grew a heterostructure for ELO-VWB, InAs layer (500 nm)/sacrificial layer/InAs buffer layer (2500 nm)/semi-insulating GaAs(001), where the sacrificial layer is a composite one, $In_{0.3}Al_{0.7}As$ (1 nm)/AlAs (2 nm)/$In_{0.3}Al_{0.7}As$ (1 nm). Using the heterostructure, the top InAs layer was transferred onto a host low-k flexible substrate, polyethylene terephthalate (PET) coated by bisazide-rubber, by ELO using HF selective wet-etching of the sacrificial layer and "inverted" VWB process as in the previous work.[11] We fabricated Hall-bar devices with current flowing direction $[1\bar{1}0]$ using the InAs films on the flexible substrate, with resist patterning of the active regions for wet recess etch-thinning. Repeating thinning by H_3PO_4-based wet-etchant, InAs thickness measurements, and Hall measurements at room temperature, we obtained the electron mobility μ and sheet concentration n_s as functions of InAs thickness L, where the measurements were carried out within several hours after the etch-thinning. The InAs thickness L was determined by confocal laser scanning microscope (CLSM) measurements using the 408-nm wavelength light, with cross-checking by atomic force microscope (AFM). Although there may be a natural surface oxide of $\sim$ nm, we do not employ a thickness correction for the natural oxidation. Figure 1(a) shows an optical microscope picture of a Hall-bar device with an InAs active region of

a)Author to whom correspondence should be addressed. Electronic mail: tosikazu@jaist.ac.jp.

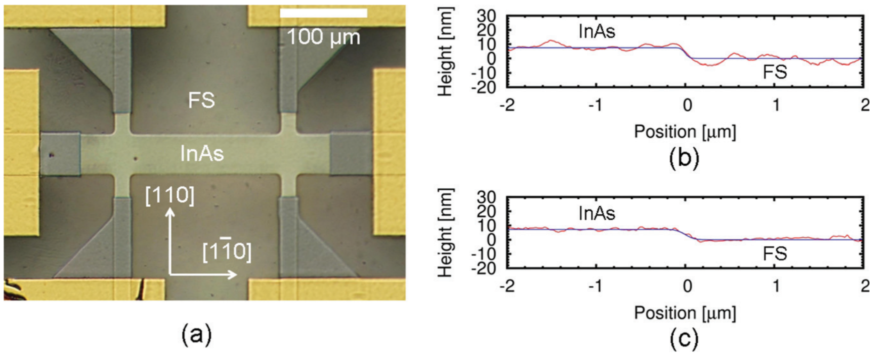

FIG. 1. An optical microscope picture (a) of a Hall-bar device on a low-*k* flexible substrate (FS), with an InAs active region of sub-10-nm thickness. Cross sectional profiles measured by CLSM (b) and AFM (c) with fitting by Gauss error functions giving thicknesses of 7.5 and 7.3 nm, respectively.

sub-10-nm thickness. The cross sectional profiles measured by CLSM and AFM are shown in Figs. 1(b) and 1(c), with fitting by Gauss error functions giving thicknesses of 7.5 and 7.3 nm, respectively. For sub-10-nm thicknesses, we cannot neglect measurement errors, in particular, those by interference effects shown in Fig. 1(b). We estimated error bars by computing variances in cross sectional profiles. The root mean square of the InAs surface roughness obtained by the AFM measurements is $\sim$1.5 nm, which is related to the thickness fluctuation. The Hall measurements were carried out under dark condition at room temperature. Because of transient changes in electron transport properties of very thin films after the light shielding, probably by trapping of photo-excited carriers, the measurements were carried out after reaching the stability. Since low temperature measurements unfortunately tend to cause sample damages due to the thermal expansion coefficient difference between InAs and the host substrate, we restricted the measurements to room temperature. In Fig. 2, L dependence of μ for many samples is shown, with the inset exhibiting L dependence of n_s. In spite of the undoped InAs films, we do not observe electron depletion even for sub-10-nm L, owing to the Fermi level pinning above the conduction band bottom.[26,27] Although n_s exhibits a variation from sample to sample for small thicknesses, μ shows more systematic behavior; we observed three regimes of μ with decrease in L. First, for $\gtrsim 150$ nm, almost constant or slightly increasing μ with decrease in L is observed. Second, we observe weakly decreasing μ for $150\,\text{nm} \gtrsim L \gtrsim 15\,\text{nm}$, where the behavior is well-fitted by

$$\mu = \left(\frac{1}{\mu_0} + \frac{1}{AL}\right)^{-1} \tag{1}$$

with $\mu_0 \simeq 15000\,\text{cm}^2/\text{V-s}$ and $A \simeq 5.3 \times 10^9\,\text{cm/V-s}$, as shown in Fig. 2. Third and last, μ decreases more rapidly as

$$\mu \propto L^{\gamma} \quad (\gamma \simeq 5\text{–}6) \tag{2}$$

for $L \lesssim 15$ nm.

In order to elucidate the behavior of the mobility μ depending on the InAs thickness L, we carried out Poisson-Schrödinger calculation,[28] where the system is modeled as an InAs film with confinement by the vacuum from the top and the bottom. The calculation is at 300 K with changing L, assuming the Fermi level and the donor concentration to reproduce n_s given by the solid curve in the inset of Fig. 2. We employed a non-parabolic electron effective mass using the non-parabolicity parameter $\alpha = 2.7\,\text{eV}^{-1}$, which becomes important for $L \lesssim 30$ nm. We calculated quantized electron energy levels E_i of i-th excited states ($i = 0, 1, 2, \ldots$), measured from the surface conduction band bottom, as functions of L, and the electron sheet concentration n_i in the i-th subband, where $\sum_i n_i = n_s$. Figure 3 shows the

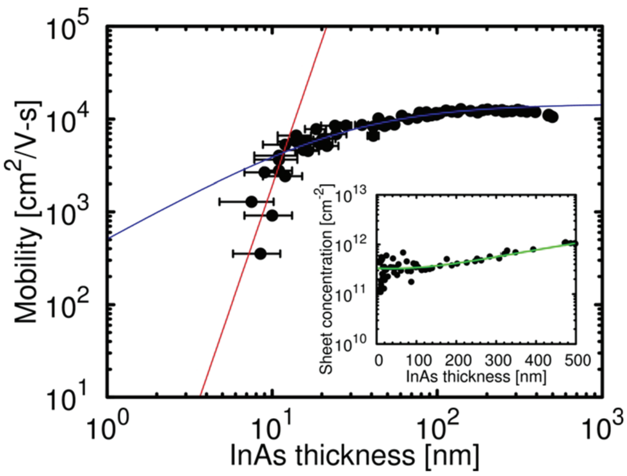

FIG. 2. The room-temperature electron mobility μ as a function of InAs thickness L for many samples, exhibiting three regimes with decrease in L. (i) Almost constant or slightly increasing μ with decrease in L for $\gtrsim 150$ nm. (ii) Weak decreasing μ, well-fitted by $\mu = (1/\mu_0 + 1/AL)^{-1}$ with $\mu_0 \simeq 15000\,\text{cm}^2/\text{V-s}$ and $A \simeq 5.3 \times 10^9\,\text{cm/V-s}$ (blue curve), for $150\,\text{nm} \gtrsim L \gtrsim 15\,\text{nm}$. (iii) Rapidly decreasing $\mu \propto L^{\gamma} (\gamma \simeq 5\text{–}6)$ (red line) for $L \lesssim 15$ nm. Inset: the sheet concentration n_s as a function of L.

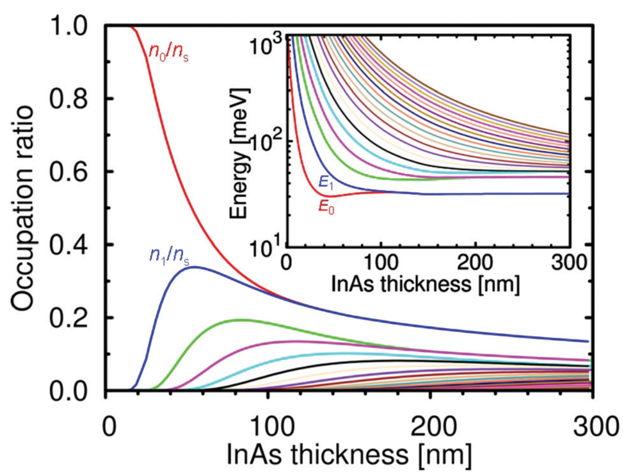

FIG. 3. The electron occupation ratio n_i/n_s (from above $i = 0, 1, 2, \ldots$), where n_s and n_i are the total and the i-th subband sheet concentration, respectively. Inset: the calculated quantized electron energy levels E_i (from below $i = 0, 1, 2, \ldots$), measured from the surface conduction band bottom.

electron occupation ratio n_i/n_s with the inset for the energy levels E_i. Figures 4(a)–4(d) show the bandbending and the electron distribution along the thickness direction in the InAs film of $L = 200$, 100, 50, and 10 nm, respectively. The position along the thickness direction is denoted by z with the origin at the center of the thickness, giving the film region of the interval $[-L/2, L/2]$ from the top to the bottom. The electron distribution is given by the electron density $\rho(z) = \sum_i \rho_i(z) = \sum_i n_i|\psi_i(z)|^2$, where $\psi_i(z)$ is the eigen wavefunction of the i-th state. Not only the total electron density $\rho(z)$ but also the ground subband electron density $\rho_0(z)$ and the 1st excited subband electron density $\rho_1(z)$ are shown.

In the first regime, as shown in Fig. 4(a), the electron distribution exhibits two peaks near the top and bottom surfaces, owing to two main independent conduction electron layers corresponding to $\rho_0(z)$ and $\rho_1(z)$ given by the degenerate ground and 1st excited states shown in the inset of Fig. 3. The distance between the top (bottom) surface and the peak of $\rho_0(z)$ ($\rho_1(z)$) is almost independent of L. Since the electron transport is mainly dominated by these two independent layers, we expect no intrinsic L dependence; the observed slight increase in μ with decrease in L is attributed to dislocation density distributions along the growth direction.[11,29]

On the other hand, in the second regime, the two layers are coupled to each other as shown in Figs. 4(b) and 4(c), indicating that the system takes on a nature of one quantum well. Although the electron distribution still exhibits two peaks near the surfaces, both $\rho_0(z)$ and $\rho_1(z)$ are spread inside the film, where the degeneracy is lifted as shown in the inset of Fig. 3. This second regime gives the L-dependent μ described by Eq. (1), indicating two mobility components; one is a constant $\mu_0 \simeq 15000\,\mathrm{cm^2/V\text{-}s}$ due to an L-independent scattering probability, and the other is an L-proportional AL with $A \simeq 5.3 \times 10^9\,\mathrm{cm/V\text{-}s}$ due to a $1/L$-proportional scattering probability. The former is attributed mainly to scattering by polar optical phonons giving a mobility of $25000\,\mathrm{cm^2/V\text{-}s}$ at room temperature[30] and to possible additional scattering such as by dislocations. For the latter, there are several possibilities. One possibility is scattering by acoustic phonons; the scattering probability between the i and j-th subbands is obtained from the square of the absolute value of the matrix element[31]

$$|M_{\mathrm{AP}}|^2 = \frac{D^2 k_{\mathrm{B}} T F_{ij}}{\rho_{\mathrm{m}} v^2} \quad \text{with} \quad F_{ij} = \int_{-L/2}^{L/2} |\psi_i(z)|^2 |\psi_j(z)|^2 \mathrm{d}z, \tag{3}$$

using the temperature T, the acoustic deformation potential D, the mass density ρ_{m}, and the sound velocity v. Since the scattering is isotropic and we obtain $F_{ij} \sim 1/L$ for the calculated wavefunctions $\psi_i(z)$, the corresponding mobility is $\mu_{\mathrm{AP}} \simeq e\hbar^3/m^{*2}|M_{\mathrm{AP}}|^2 \sim AL$, where m^* is the electron effective mass. However, the value of A is estimated to be $\gtrsim 10^{11}\,\mathrm{cm/V\text{-}s}$ for bulk InAs, which seems too large in comparison with the observed value $\simeq 5.3 \times 10^9\,\mathrm{cm/V\text{-}s}$. Another possibility is Coulomb scattering by random charges at the surfaces, which is expected to have significant effects in the system obtained by ELO-VWB. The i-th intrasubband scattering probability due to the top surface charge at $z = -L/2$ is obtained from the square of the absolute value of the matrix element[18,19,32]

$$|M_{\mathrm{C}}|^2 \propto \frac{F_i(q)^2}{q^2} \ \text{with}\ F_i(q) = \int_{-L/2}^{L/2} |\psi_i(z)|^2 e^{-q(z+L/2)} \mathrm{d}z, \tag{4}$$

where q is the absolute value of the two-dimensional wavenumber change due to scattering. With k denoting the absolute value of the original two-dimensional wavenumber and θ denoting the scattering angle, we obtain $q = 2k\sin(\theta/2)$, and integrating on θ gives the scattering probability proportional to

$$\int_0^{2\pi} \frac{F_i(2k\sin(\theta/2))^2}{4k^2\sin^2(\theta/2)}(1-\cos\theta)\mathrm{d}\theta \propto \int_0^1 \frac{F_i(2ks)^2}{\sqrt{1-s^2}}\mathrm{d}s = I_i. \tag{5}$$

Figure 5(a) shows the Coulomb scattering integral I_i ($i = 0$, 1) defined by Eq. (5) as a function of L for several values of k, obtained from the calculated wavefunctions $\psi_i(z)$. We find

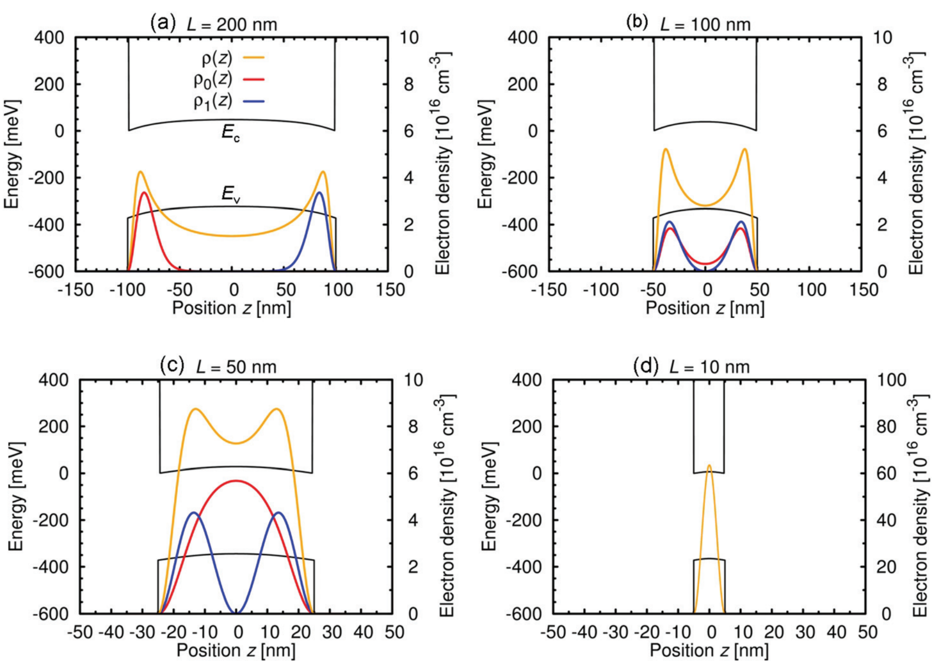

FIG. 4. The calculated bandbending along the thickness direction in the InAs film with thickness of (a) L=200 nm, (b) 100 nm, (c) 50 nm, and (d) 10 nm, with the total electron density $\rho(z)$, the ground subband electron density $\rho_0(z)$, and the 1st excited subband electron density $\rho_1(z)$.

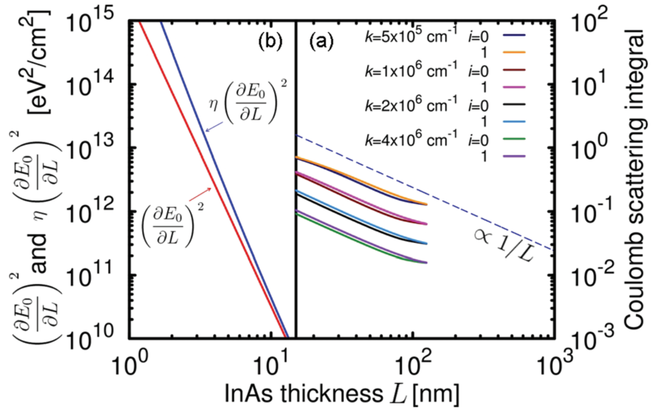

FIG. 5. (a) The Coulomb scattering integral I_i $(i = 0, 1)$ defined by Eq. (5) proportional to scattering probability for $k = 5 \times 10^5$, 1×10^6, 2×10^6, and 4×10^6 cm^{-1}, showing $1/L$ behavior. (b) $(\partial E_0/\partial L)^2$ proportional to thickness fluctuation scattering probability, showing $1/L^{4.9}$ behavior, and $\eta(\partial E_0/\partial L)^2$ proportional to the reciprocal mobility, showing $1/L^{5.2}$ behavior, where $\eta = m^*(E_0)/m^*(0)$.

$I_i \simeq 1/2kL \propto 1/L$ and the corresponding mobility $\mu_C \propto L$. Moreover, from the observed $A \simeq 5.3 \times 10^9$ cm/V-s, we can estimate the surface random charge density $\lesssim 10^{12}$ cm^{-2}, which seems a reasonable value. Therefore, the surface charge Coulomb scattering is a plausible contributing mechanism in the second regime.

In the third regime, as shown in Fig. 4(d), the system is a narrow quantum well with a strong confinement and a single-peaked electron distribution, where almost only the ground subband is occupied by electrons. The observed μ described by Eq. (2) indicates that the thickness fluctuation scattering is dominant,[18–23] which can be described by a perturbation Hamiltonian approach.[22] With a thickness L and a center position z_0, let $\mathcal{H}(z) = \mathcal{H}_K + V$ be the Hamiltonian of the film, where $\mathcal{H}_K = -\hbar^2\partial_z^2/2m^*$ is the kinetic term and $V = V(z)$ is the potential term. By a thickness fluctuation δL and a center position fluctuation Δ, i.e., $L \to L + \delta L$ and $z_0 \to z_0 + \Delta$, we obtain the modified Hamiltonian $\tilde{\mathcal{H}}(z) = \mathcal{H}((z - \Delta)L/(L + \delta L))$. Therefore, we obtain the perturbation Hamiltonian in the first order

$$\Delta\mathcal{H} = \frac{\partial\mathcal{H}}{\partial L}\delta L + \frac{\partial\mathcal{H}}{\partial z_0}\Delta = \frac{\hbar^2\partial_z^2}{m^*}\frac{\delta L}{L} - z\frac{\partial V}{\partial z}\frac{\delta L}{L} - \frac{\partial V}{\partial z}\Delta, \quad (6)$$

where the first term gives the confinement energy fluctuation with the so-called sixth-power thickness law of the mobility. Since the last term is negligible in our system due to the symmetry, for the intrasubband scattering, the perturbation gives the square of the absolute value of the matrix element $|\langle\psi_i|\partial\mathcal{H}/\partial L|\psi_i\rangle|^2\delta L^2 = (\partial E_i/\partial L)^2\delta L^2$, where the Hellmann-Feynman theorem is used. Figure 5(b) shows the behavior of $(\partial E_0/\partial L)^2$ and $\eta(\partial E_0/\partial L)^2$, where $\eta = m^*(E_0)/m^*(0)$ is relative effective mass due to the non-parabolicity. The latter is proportional to the reciprocal mobility, showing $1/L^{5.2}$ behavior, which is in agreement with the observation, where the exponent can be smaller than 6 owing to the non-parabolicity effects. We observe a strong scattering attributed to a large thickness fluctuation in the films obtained by ELO-VWB, as suggested by the observed root mean square roughness, and to the small electron effective mass of InAs.

In summary, we investigated InAs films with thickness ranging from several hundreds of nm to sub-10-nm, obtained by ELO-VWB on low-k flexible substrates. We observed three regimes of the behavior of electron mobility with decrease in thickness. By using Poisson-Schrödinger calculation, we examined the electron distribution and the associated scattering mechanisms contributing to the behavior of the mobility. As a result, the importance of the surface charge Coulomb scattering and the thickness fluctuation scattering is manifested.

[1]A. Milnes and A. Polyakov, Mater. Sci. Eng. B **18**, 237 (1993).
[2]H. Kroemer, Physica E **20**, 196 (2004).
[3]Z. Yin and X. Tang, Solid-State Electron. **51**, 6 (2007).
[4]B. R. Bennett, R. Magno, J. B. Boos, W. Kruppa, and M. G. Ancona, Solid-State Electron. **49**, 1875 (2005).
[5]D.-H. Kim and J. del Alamo, IEEE Electron Device Lett. **31**, 806 (2010).
[6]N. Li, E. S. Harmon, J. Hyland, D. B. Salzman, T. P. Ma, Y. Xuan, and P. D. Ye, Appl. Phys. Lett. **92**, 143507 (2008).
[7]Q. Zhang, W. Zhao, and A. Seabaugh, IEEE Electron Device Lett. **27**, 297 (2006).
[8]M. Luisier and G. Klimeck, IEEE Electron Device Lett. **30**, 602 (2009).
[9]Y. Jeong, M. Shindo, M. Akabori, and T. Suzuki, Appl. Phys. Express **1**, 021201 (2008).
[10]Y. Jeong, M. Shindo, H. Takita, M. Akabori, and T. Suzuki, Phys. Stat. Sol. C **5**, 2787 (2008).
[11]H. Takita, N. Hashimoto, C. T. Nguyen, M. Kudo, M. Akabori, and T. Suzuki, Appl. Phys. Lett. **97**, 012102 (2010).
[12]M. Konagai, M. Sugimoto, and K. Takahashi, J. Cryst. Growth **45**, 277 (1978).
[13]E. Yablonovitch, T. Gmitter, J. P. Harbison, and R. Bhat, Appl. Phys. Lett. **51**, 2222 (1987).
[14]J. Shi, N. Wichmann, Y. Roelens, and S. Bollaert, Appl. Phys. Lett. **99**, 203505 (2011).
[15]H. Ko, K. Takei, R. Kapadia, S. Chuang, H. Fang, P. W. Leu, K. Ganapathi, E. Plis, H. S. Kim, S.-Y. Chen, M. Madsen, A. C. Ford, Y.-L. Chueh, S. Krishna, S. Salahuddin, and A. Javey, Nature (London) **468**, 286 (2010).
[16]K. Takei, S. Chuang, H. Fang, R. Kapadia, C.-H. Liu, J. Nah, H. S. Kim, E. Plis, S. Krishna, Y.-L. Chueh, and A. Javey, Appl. Phys. Lett. **99**, 103507 (2011).
[17]K. Takei, H. Fang, S. B. Kumar, R. Kapadia, Q. Gao, M. Madsen, H. S. Kim, C.-H. Liu, Y.-L. Chueh, E. Plis, S. Krishna, H. A. Bechtel, J. Guo, and A. Javey, Nano Lett. **11**, 5008 (2011).
[18]A. Gold, Solid State Commun. **60**, 531 (1986).
[19]A. Gold, Phys. Rev. B **35**, 723 (1987).
[20]H. Sakaki, T. Noda, K. Hirakawa, M. Tanaka, and T. Matsusue, Appl. Phys. Lett. **51**, 1934 (1987).
[21]C. R. Bolognesi, H. Kroemer, and J. H. English, Appl. Phys. Lett. **61**, 213 (1992).
[22]T. Ishihara, K. Uchida, J. Koga, and S. Takagi, Jpn. J. Appl. Phys. **45**, 3125 (2006).
[23]A. Gold, J. Appl. Phys. **103**, 043718 (2008).
[24]K. Uchida and S. Takagi, Appl. Phys. Lett. **82**, 2916 (2003).
[25]M. Yokoyama, R. Iida, S. Kim, N. Taoka, Y. Urabe, H. Takagi, T. Yasuda, H. Yamada, N. Fukuhara, M. Hata, M. Sugiyama, Y. Nakano, M. Takenaka, and S. Takagi, IEEE Electron Device Lett. **32**, 1218 (2011).
[26]L. Ö. Olsson, C. B. M. Andersson, M. C. Håkansson, J. Kanski, L. Ilver, and U. O. Karlsson, Phys. Rev. Lett. **76**, 3626 (1996).
[27]H. Yamaguchi, R. Dreyfus, Y. Hirayama, and S. Miyashita, Appl. Phys. Lett. **78**, 2372 (2001).
[28]G. L. Snider, *Computer Program 1D Poisson/Schrödinger: A Band Diagram Calculator* (University of Notre Dame, Notre Dame, Indiana, 1995).
[29]Y. Jeong, H. Choi, and T. Suzuki, J. Cryst. Growth **301–302**, 235 (2007).
[30]T. Suzuki, H. Ono, and S. Taniguchi, Sci. Technol. Adv. Mater. **6**, 400 (2005).
[31]P. J. Price, Ann. Phys. **133**, 217 (1981).
[32]T. H. Ning and C. T. Sah, Phys. Rev. B **6**, 4605 (1972).